

後も小腸病変のサーベイランスが重要であり、GSを容易かつ確実な観察するために、Billroth I法再建としている。

これまで、FAPに随伴するDPに対して、腹腔鏡下にPPTDを施行した報告もある^{2,3)}が、一般的に十分に普及した術式とはいえない。当科では腹腔鏡を用いない低侵襲手術として、6~7 cmの小切開による幽門側胃切除術⁵⁾や結腸癌根治術を行い、その手術手技⁶⁾や低侵襲性⁷⁾などについて報告してきた。小切開下手術は、腹腔鏡(補助)下手術と比べてコスト削減だけでなく、専門的に修練された限られた外科医でなくとも安全に確実な手術が可能であることを述べてきた。それらの経験を生かして今回、小切開下のPPTDを施行したが、報告されている腹腔鏡下のPPTDに比べて手術時間、術中出血量、術後合併症などに関して勝るとも劣らない結果であり、安全、確実な手術操作が可能であった。

また、今回の症例は術後6か月において、開腹創およびドレーン刺入創の肥厚性瘢痕を認めた。FAPに随伴するデスモイド腫瘍の原因の一つとして、創傷に伴う肥厚性瘢痕が指摘されており⁸⁾、今回の症例において肥厚性瘢痕を来しやすい手術創を結果的に小さくすることができたという点から、小切開下手術はよい適応であったと思われる。特に今回の症例のような若年女性のFAPに随伴する十二指腸ポリープシスに対する小切開下のPPTDは、安全性かつ整容性の面においても許容されるものと考えられた。

結 語

今回われわれは、家族性大腸腺腫症に随伴する十二指腸ポリープシスに対して、小切開下に腓温存全十二指腸切除術を施行した。

文 献

- 1) Rustgi AK: Hereditary gastrointestinal polyposis and nonpolyposis syndromes. *N Engl J Med* 331(25):1694-1702, 1994.
- 2) Stauffer JA, Adkisson CD, Riegert-Johnson DL, et al: Pancreas-sparing total duodenectomy for ampullary duodenal neoplasms. *World J Surg* 36(10):2461-2472, 2012.
- 3) Benetatos N, Ammori MB and Ammori BJ: Laparoscopic pancreas-preserving total duodenectomy for familial adenomatous polyposis. *Surg Laparosc Endosc Percutan Tech* 21(6):e332-e335, 2011.
- 4) Ishikawa H, Mutoh M, Iwama T, et al: Endoscopic management of familial adenomatous polyposis in patients refusing colectomy. *Endoscopy*: 2015. [Epub ahead of print]
- 5) Ishida H, Ishiguro T, Miyazaki T, et al: Distal gastrectomy via minilaparotomy for non-overweight patients with T1N0-1 gastric cancer: initial experience of 30 cases. *Int J Surg* 8(8):643-647, 2010.
- 6) Ishida H, Ishiguro T, Ishibashi K, et al: Impact of prior abdominal surgery on curative resection of colon cancer via minilaparotomy. *Surg Today* 41(3):369-376, 2011.
- 7) Ishida H, Nakada H, Yokoyama Y, et al: Minilaparotomy approach for colonic cancer: initial experience of 54 cases. *Surg Endosc* 19(3):316-320, 2005.
- 8) Carothers AM, Rizvi H, Hasson RM, et al: Mesenchymal stromal cell mutations and wound healing contribute to the etiology of desmoid tumors. *Cancer Res* 72(1):346-355, 2012.

本論文の要旨は第37回日本癌局所療法研究会において発表した。

家族性大腸腺腫症に発生した子宮内膜癌, 卵巣癌, 十二指腸癌の1例

石橋敬一郎 渡辺雄一郎 近 範 泰 田島 雄介 鈴木 興秀
 松澤 岳晃 隈元 謙介 福地 稔 熊谷 洋一 馬場 裕之
 持木 彫人 岩間 毅夫 石田 秀行*

(*Jpn J Cancer Chemother* 42(12): 1715-1717, November, 2015)

A Case of Carcinoma of the Uterine Body, Right Ovary, and Duodenum in a Patient with Familial Adenomatous Polyposis: Keiichiro Ishibashi, Yuichiro Watanabe, Noriyasu Chika, Yusuke Tajima, Okihide Suzuki, Takeaki Matsuzawa, Kensuke Kumamoto, Minoru Fukuchi, Yoichi Kumagai, Hiroyuki Baba, Erito Mochiki, Takeo Iwama and Hideyuki Ishida (Dept. of Digestive Tract and General Surgery, Saitama Medical Center, Saitama Medical University)

Summary

We report a case of 4 carcinomas of the uterine body, right ovary, and duodenum in a patient with familial adenomatous polyposis (FAP). Her mother's family line carries FAP. She underwent proctocolectomy with ileoanal anastomosis for FAP when she was 20 years old. She was diagnosed with carcinoma of the uterine body and right ovary, and underwent abdominal total hysterectomy, bilateral salpingo-oophorectomy, and omentectomy at 48 years of age. The pathological examination revealed endometrioid adenocarcinoma of the uterine body (Stage IB) and endometrioid adenocarcinoma of the right ovary (Stage IA). Her diagnosis was Stage IV according to the Spigelman classification of duodenal polyposis, and she underwent pancreas-preserving total duodenectomy at 50 years of age. The pathological examination was conclusive for 2 carcinomas in the adenoma, which were 20 mm and 25 mm in diameter, respectively. She has been well without any evidence of cancer recurrence 20 months after the pancreas-preserving total duodenectomy. Key words: Familial adenomatous polyposis, Carcinoma of duodenum, Carcinoma of the uterine body, Carcinoma of the ovary

要旨 家族性大腸腺腫症 (FAP) に対する大腸全摘, 回腸囊肛門吻合術後に子宮体癌・卵巣癌, 十二指腸癌が異時性に発生した1例を経験したので報告する。症例は48歳, 女性。母方がFAP家系。20歳時, FAPに対して大腸全摘, 回腸囊肛門吻合術を施行した。その後, 長期にわたって随伴病変のサーベイランスを行ってきた。48歳時, 子宮体癌および右卵巣腫瘍の診断で単純子宮全摘, 両側付属器切除, 大網切除術を施行した。病理診断は, 子宮体癌 (endometrioid adenocarcinoma), Stage IB, 卵巣癌 (endometrioid adenocarcinoma), Stage IAであった。50歳時, Spigelman分類 Stage IVの十二指腸ポリポーシスに対し, 腺温存全十二指腸切除術を施行した。2病変 (最大径20 mm, 25 mm) に carcinoma in adenoma, tub1, Tis, Stage 0 が認められた。腺温存十二指腸切除術から20か月経過した現在, 再発などは認めていない。大腸切除後のFAPでは, 十二指腸癌に対する長期にわたるサーベイランスが必要であるが, 婦人科癌について従来関連性は低いと考えられてきた。この点を明らかにするには症例の集積が必要である。

はじめに

家族性大腸腺腫症 (familial adenomatous polyposis: FAP) の大腸外随伴病変である十二指腸腺腫は, 40歳をすぎると合併頻度が高くなり, 最終的には90%に合併することが報告されている^{1,2)}。また, 子宮癌, 卵巣癌などの婦人科癌は一般に大腸外随伴病変でないと考えられている。

今回われわれは, FAPに対する大腸全摘, 回腸囊肛門吻合術後に子宮体癌, 卵巣癌, 十二指腸癌が異時性に発生した1例を経験したので報告する。

I. 症 例

患者: 48歳, 女性。

家族歴: 母, 兄, 娘がFAP, 母は大腸癌で42歳で死亡。娘は甲状腺癌で手術を受けている (図1)。

既往歴: 統合失調症。

現病歴: 20歳時, FAPに対して大腸全摘, 回腸囊肛門吻合術を施行した。その後, 通院加療をしていた。

下腹部MRI検査: 48歳時, 定期検査で行った下腹部MRI検査で, 子宮底部の内膜は著明に肥厚し, 不均一なT2低信号を認めた。また, 右卵巣に嚢胞性腫瘍を認め,

* 埼玉医科大学総合医療センター・消化管・一般外科

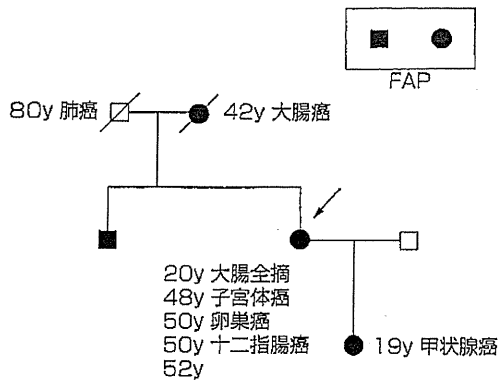


図1 家系図

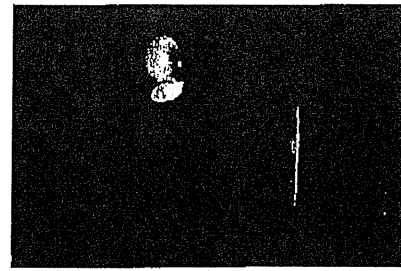


図2 下腹部MRI T2検査
子宮底部の内膜は著明に肥厚し、不均一なT2低信号を認めた。また、右卵巣に嚢胞性腫瘍を認め、一部に不整形のT2低信号を認めた。

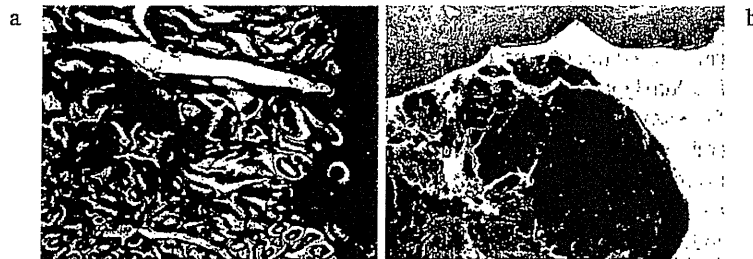


図3 子宮、卵巣病理所見
a: 子宮体癌。endometrioid adenocarcinoma, Stage IB。
b: 卵巣癌。endometrioid adenocarcinoma, Stage IA。

一部に不整形のT2低信号を認めた(図2)。

血液生化学検査:血液生化学検査に異常は認めなかった。腫瘍マーカーはCEA 3.0 ng/mL(基準値6.7 ng/mL以下), CA19-9 10 U/mL(基準値37 U/mL以下), CA125 8 U/mL(基準値35 U/mL以下)と基準値以下であった。

以上より、子宮体癌、右卵巣腫瘍(癌の疑い)の診断で、単純子宮全摘、両側付属器切除、大網切除術を施行した。

子宮・卵巣病理所見:子宮体部はexophytic type, endometrioid adenocarcinoma, Grade 1, ly(-), v(-), pT1b, pN0, Stage IBであった(図3a)。右卵巣はendometrioid adenocarcinoma, pT1a, Stage IAであった(図3b)。

上部消化管内視鏡検査:50歳時、定期的に行っていた上部消化管内視鏡検査で、十二指腸球部から水平部にかけて、20個以上の数mmから20mm大の平坦隆起のポリープを認めた。中央に陥凹を伴う扁平な腫瘍も認められた(図4)。生検では、tubulo-villous adenoma, moderate dysplasiaであり、十二指腸ポリポーシスの臨床病理分類であるSpigelman分類10点、Stage IVと診断された³⁾。

以上より、FAPに随伴する多発十二指腸腺腫症の診

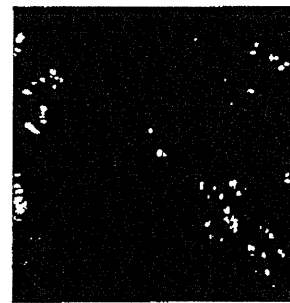


図4 上部消化管内視鏡所見
ポリープ数20個以上、大きさ10mm以上、異型度:中程度、組織構造:管状~絨毛状であり、Spigelman分類Stage IVと診断。

断で、脾温存十二指腸切除術⁴⁾を施行した。再建は残胃と空腸をBillroth I法式で吻合した。

十二指腸病理所見:20mm大、25mm大の二つの腫瘍はcarcinoma in adenoma, tub1, Tis, Stage 0(TNM分類第7版)であった。他のポリープはすべてtubular adenomaであった(図5)。

脾温存十二指腸切除術から1年8か月経過した現在、いずれの癌の再発も認めていない。

II. 考 察

FAPの大腸外随伴病変としては、胃底腺ポリポーシ



図5 十二指腸病理所見
2病変(最大径20 mm, 25 mm)は carcinoma in adenoma, tub1, Tis, Stage 0であった。

ス、胃腺腫、十二指腸ポリポシス、十二指腸乳頭部腺腫、空・回腸腺腫、デスマイド腫瘍、頭蓋骨腫、顎潜在骨腫、過剰歯、埋没歯、類上皮腫、甲状腺癌、先天性網膜色素上皮肥大、肝芽腫、副腎腫瘍、脳腫瘍などが報告されている⁵⁾。消化管以外の悪性腫瘍としては、甲状腺癌(特に女性)^{6,7)}、副腎癌^{8,9)}、肝芽腫¹⁰⁾、脳腫瘍¹¹⁾などが知られているが、子宮癌、卵巣癌はFAPの随伴病変とは考えられていない。しかし、FAPの死因について集計したIwamaらの報告¹²⁾では、1990～2003年のFAP死因の1.4%が子宮癌であった。子宮癌、卵巣癌はFAPの随伴病変ではないが、今後症例の集積とともに癌組織の生殖細胞系列変異、体細胞系列変異などを検索し、FAPとの関連を検討していくことが必要である。APC遺伝子のいわゆるtwo-hitがFAPの婦人科癌で認められるかについて、症例ごとに解析していく必要がある。

Iwamaらの報告¹²⁾では、十二指腸・乳頭部癌は1990～2003年のFAP死因の5.6%と報告されている。十二指腸腺腫は40歳をすぎると多くなり、最終的には90%に合併することが報告されている^{1,2)}。十二指腸ポリポシスの病期分類としてのSpigelman分類³⁾が広く用いられている。ポリープ数、大きさ、異型度、組織構造が点数化され、Stage 0～Vに分類されているが、Stage IVでは最終的に7～36%に癌化が認められると報告されている^{13,14)}。Stage IVでは、外科治療を念頭に置いた6～12か月ごとの内視鏡検査、手術(幽門輪温存膵頭十二指腸切除、膵温存全十二指腸切除など)が推奨されている。Spigelman分類Stage IV十二指腸ポリポシスに対する膵温存全十二指腸切除術¹⁵⁾は、膵頭十二指腸切除術や幽門輪温存膵頭十二指腸切除術に比べて、比較的安全に施行でき、術後糖尿病や脂肪肝発生のリスクがないので、「予防的十二指腸切除」の観点から有用な術式と考えられる。

文 献

- 1) Moozar KL, Madlensky L, Berk T, *et al*: Slow progression of periampullary neoplasia in familial adenomatous polyposis. *J Gastrointest Surg* 6(6): 831-837, 2002.
- 2) Brosens LA, Keller JJ, Offerhaus GJ, *et al*: Prevention and management of duodenal polyps in familial adenomatous polyposis. *Gut* 54(7): 1034-1043, 2005.
- 3) Spigelman AD, Williams CB, Talbot IC, *et al*: Upper gastrointestinal cancer in patients with familial adenomatous polyposis. *Lancet* 2(8666): 783-785, 1989.
- 4) Chung RS, Church JM and vanStolk R: Pancreas-sparing duodenectomy: indications, surgical technique, and results. *Surgery* 117(3): 254-259, 1995.
- 5) 大腸癌研究会/編: 遺伝性大腸癌診療ガイドライン. 2012年版, 金原出版, 東京, 2012.
- 6) Iwama T, Mishima Y and Utsunomiya J: The impact of familial adenomatous polyposis on the tumorigenesis and mortality at the several organs. Its rational treatment. *Ann Surg* 217(2): 101-108, 1993.
- 7) Giardiello FM, Offerhaus GJ, Lee DH, *et al*: Increased risk of thyroid and pancreatic carcinoma in familial adenomatous polyposis. *Gut* 34(10): 1394-1396, 1993.
- 8) Smith TG, Clark SK, Katz DE, *et al*: Adrenal masses are associated with familial adenomatous polyposis. *Dis Colon Rectum* 43(12): 1739-1742, 2000.
- 9) Marchesa P, Fazio VW, Church JM, *et al*: Adrenal masses in patients with familial adenomatous polyposis. *Dis Colon Rectum* 40(9): 1023-1028, 1997.
- 10) Hughes LJ and Michels VV: Risk of hepatoblastoma in familial adenomatous polyposis. *Am J Med Genet* 43(6): 1023-1025, 1992.
- 11) Hamilton SR, Liu B, Parsons RE, *et al*: The molecular basis of Turcot's syndrome. *N Engl J Med* 332(13): 839-847, 1995.
- 12) Iwama T, Tamura K, Morita T, *et al*: A clinical overview of familial adenomatous polyposis derived from the database of the Polyposis Registry of Japan. *Int J Clin Oncol* 9(4): 308-316, 2004.
- 13) Groves CJ, Saunders BP, Spigelman AD, *et al*: Duodenal cancer in patients with familial adenomatous polyposis (FAP): results of a 10 year prospective study. *Gut* 50(5): 636-641, 2002.
- 14) Iida M, Yao T, Itoh H, *et al*: Natural history of duodenal lesions in Japanese patients with familial adenomatous polyposis coli (Gardner's syndrome). *Gastroenterology* 96(5 Pt 1): 1301-1306, 1989.
- 15) Chung RS, Church JM and vanStolk R: Pancreas-sparing duodenectomy: indications, surgical technique, and results. *Surgery* 117(3): 254-259, 1995.

本論文の要旨は第37回日本癌局所療法研究会において発表された。

1) Moozar KL, Madlensky L, Berk T, *et al*: Slow progression of periampullary neoplasia in familial adenomatous poly-

Long-term outcomes after treatment for pedunculated-type T1 colorectal carcinoma: a multicenter retrospective cohort study

Naoki Asayama¹ · Shiro Oka¹ · Shinji Tanaka¹ · Shinji Nagata² · Akira Furudo³ · Toshio Kuwai⁴ · Seiji Onogawa⁵ · Tadamasa Tamura⁶ · Hiroyuki Kanao⁷ · Yuko Hiraga⁸ · Hideharu Okanobu⁹ · Takayasu Kuwabara¹⁰ · Masaki Kunihiro¹¹ · Shinichi Mukai¹² · Eizo Goto¹³ · Fumio Shimamoto¹⁴ · Kazuaki Chayama¹⁵

Received: 7 September 2015 / Accepted: 31 October 2015
© Japanese Society of Gastroenterology 2015

Abstract

Background The risk for lymph node metastasis and the prognostic significance of pedunculated-type T1 colorectal carcinomas (CRCs) require further study. We aimed to assess the validity of the 2014 Japanese Society for Cancer of the Colon and Rectum (JSCCR) guidelines based on long-term outcomes of pedunculated-type T1 CRCs.

Methods In this multicenter retrospective cohort study, we examined 176 patients who underwent resection endoscopically or surgically at 14 institutions between January 1990 and December 2010. Patients meeting the JSCCR curative criteria were defined as “endoscopically curable (e-curable)” and those who did not were “non-e-curable”. We evaluated the prognosis of 116 patients (58 e-curable, 58 non-e-curable) who were observed for >5 years after treatment.

Results Overall incidence of lymph node metastasis was 5 % (4/81; 95 % confidence interval 1.4–12 %: three cases of submucosal invasion depth ≥ 1000 μm [stalk invasion] and lymphatic invasion, one case of head invasion and budding grade 2/3). There was no local or metastatic recurrence in the e-curable patients, but six of them died of another cause (observation period, 80 months). There was no local recurrence in the non-e-curable patients; however, distant metastasis was observed in one patient. Death due to the primary disease was not observed in non-e-curable patients, but six of them died of another cause (observation period, 72 months).

Conclusions Our data support the validity of the JSCCR curative criteria for pedunculated-type T1 CRCs. Endoscopic resection cannot be considered curative for pedunculated-type T1 CRC with head invasion alone.

✉ Shiro Oka
oka4683@hiroshima-u.ac.jp

¹ Department of Endoscopy, Hiroshima University Hospital, Hiroshima, Japan

² Department of Gastroenterology, Hiroshima City Asa Citizens Hospital, Hiroshima, Japan

³ Department of Gastroenterology, JA Hiroshima General Hospital, Hiroshima, Japan

⁴ Department of Gastroenterology, National Hospital Organization Kure Medical Center and Chugoku Cancer Center, Hiroshima, Japan

⁵ Department of Gastroenterology, Onomichi General Hospital, Hiroshima, Japan

⁶ Department of Internal Medicine, Hiroshimakenin Hospital, Hiroshima, Japan

⁷ Department of Gastroenterology, Hiroshima Red Cross Hospital and Atomic-bomb Survivors Hospital, Hiroshima, Japan

⁸ Department of Endoscopy, Hiroshima Prefectural Hospital, Hiroshima, Japan

⁹ Department of Gastroenterology, Chugoku Rosai Hospital, Hiroshima, Japan

¹⁰ Department of Gastroenterology, Shobara Red Cross Hospital, Hiroshima, Japan

¹¹ Department of Internal Medicine, Hiroshima City Hiroshima Citizens Hospital, Hiroshima, Japan

¹² Department of Gastroenterology, Miyoshi Central Hospital, Hiroshima, Japan

¹³ Department of Gastroenterology, Higashihiroshima Medical Center, Hiroshima, Japan

¹⁴ Department of Health Science, Faculty of Human Culture and Science, Prefectural University of Hiroshima, Hiroshima, Japan

¹⁵ Department of Gastroenterology and Metabolism, Hiroshima University Hospital, Hiroshima, Japan

Keywords Pedunculated-type T1 colorectal carcinoma · Lymph node metastasis · Clinicopathological characteristics · Outcomes

Introduction

As a result of recent advances in endoscopic instruments and techniques, the proportion of T1 colorectal carcinoma (CRC) initially treated by endoscopic resection (ER) has been increasing [1–5]. However, lymph node (LN) metastasis occurs in approximately 10 % of T1 CRCs [4–8]; furthermore, the rate of LN metastasis is reportedly 3.5–7.5 % in pedunculated-type T1 CRC [9–17]. Despite the low incidence of LN metastasis, surgical resection with regional LN dissection is considered the standard treatment for T1 CRC [18]. According to the Japanese Society for Cancer of the Colon and Rectum (JSCCR) guidelines, the curative criteria for T1 CRC after ER are well/moderately differentiated or papillary carcinoma, no vascular invasion, submucosal (SM) invasion depth <1000 μ m, and budding grade 1, because of the very low risk of LN metastasis associated with these pathological features [19].

In Western countries, Haggitt's classification is frequently used to define the depth of invasion of pedunculated-type T1 CRC [20]. Haggitt and colleagues stratified the level of carcinoma invasion according to the following criteria: level 0, carcinoma in situ (i.e., no extension below the muscularis mucosae); level 1, invasion through the muscularis mucosae but limited to the head of the polyp (i.e., above the junction between the adenoma and its stalk); level 2, invasion at the level of the neck (i.e., the junction between the adenoma and its stalk); level 3, invasion of any part of the stalk; and level 4, invasion into the submucosa of the bowel wall below the stalk. The authors concluded that the risk of metastasis or local recurrence is low when the level is <4.

A project conducted by JSCCR reported a rate of LN metastasis of 0 % in pedunculated T1 CRCs with invasion above the boundary of Haggitt's level 2 (Haggitt's line) and in those that had invaded beyond Haggitt's line to a SM depth of <3000 μ m with no lymphatic invasion [14]. In a retrospective multicenter study that enrolled 384 pedunculated-type T1 CRC patients treated by ER or surgical resection, Matsuda et al. concluded that all cases with LN metastasis or recurrence were in those with carcinoma that had invaded beyond Haggitt's line [15]. Several studies have reported long-term outcomes for T1 CRCs treated with ER [13, 21–25]; however, the JSCCR guidelines do not clearly outline the long-term outcomes of patients with T1 CRC who underwent ER or surgical

resection. Compared with non-pedunculated T1 CRCs, pedunculated-type T1 CRCs tend to be easier to detect, diagnose, and treat by initial ER as total excisional biopsy [3]. However, the risk of LN metastasis and the prognostic significance of pedunculated-type T1 CRCs have not been studied adequately. This study aimed to assess the clinical validity of the JSCCR guidelines based on long-term outcomes for pedunculated-type T1 CRCs after ER or surgical resection.

Patients and methods

Patients

We evaluated the clinicopathological characteristics of 176 patients with 176 pedunculated-type T1 CRCs [138 (78 %) men, mean age 64 (range, 29–84) years, median follow-up period 105.5 months] resected endoscopically or surgically at Hiroshima University Hospital and 13 affiliated hospitals between January 1990 and December 2010. Patients who met the JSCCR curative criteria were defined as “endoscopically curable (e-curable)” and those who did not were defined as “non-e-curable”. We also evaluated the prognosis of the 116 patients (58 e-curable, 58 non-e-curable) who were followed up for >5 years after treatment, with a mean follow-up duration of 124 ± 77 months. Patients who were eligible for this study had pathologically proven adenocarcinoma invading through the muscularis mucosae into the SM layer but not extending deeply into the muscularis propria. Patients with previous or synchronous advanced CRC; multiple, early, invasive CRCs; inflammatory bowel disease; hereditary non-polyposis CRC; and familial adenomatous polyposis were excluded from this study. Patients who underwent surgical resection without LN dissection (transanal endoscopic microsurgery and local resection) as initial treatment for T1 CRC were also excluded. The study protocol was approved by the Ethics Committee of Hiroshima University and complied with the guidelines of the Ministry of Health, Labour and Welfare of the Japanese Government.

Indication and procedure for ER

ER methods consist of polypectomy or endoscopic mucosal resection. Patients enrolled in this study were treated according to the JSCCR guidelines [19], which specify that ER should not be applied for early CRC if en bloc removal is impossible or for clinical T1 CRC with deep invasion of the submucosa prior to treatment.

Indications for additional surgical treatment after ER

The JSCCR guidelines state that a positive deep tumor margin is an absolute indication for additional surgery after ER. Additional surgical treatment after ER should be considered when at least one of the following is found: (1) SM invasion depth ≥ 1000 μm ; (2) positive vascular invasion; (3) poorly differentiated adenocarcinoma, signet ring cell carcinoma, or mucinous carcinoma; and (4) budding grade 2/3 at the deepest part of SM invasion [19]. A budding is defined as a single cancer cell or a cluster of <5 cells along the invasion margin, and budding is graded per microscopic field at $200\times$ magnification (i.e., grade 1, 0–4; grade 2, 5–9; grade 3, ≥ 10 buds) [7].

The JSCCR guidelines clearly state that additional surgical treatment should be performed only after systematically evaluating the predicted curability based on various LN metastasis risk factors and the patient's condition (age, physical performance, and presence of adverse event, etc.) and after obtaining informed consent from the patients [19].

Method for measuring depth of SM invasion

According to the JSCCR guidelines [19], the method used for measurement of SM depth is as follows. When it is possible to identify or estimate the location of the muscularis mucosae, the depth of SM invasion is measured from the lower border of the muscularis mucosae of the lesion, irrespective of macroscopic type. When it is not possible to identify or estimate the location of the muscularis mucosae, the depth of SM invasion is measured from the surface of the lesion. The phrase “possible to identify or to estimate” means that there is no “deformity”, that is, no disarray, dissection, rupture, fragmentation, etc., of the muscularis mucosae as a result of SM invasion. If a deformed muscularis mucosa is used as the measurement baseline, the depth of SM invasion may be underestimated. Although judging whether deformity is present is not always straightforward, if a desmoplastic reaction is present around the muscularis mucosae, it is assumed to be “deformed”. For pedunculated-type CRCs with a tangled muscularis mucosae, the depth of SM invasion is measured from Haggitt's line. Invasion within the head alone is defined as “head invasion”.

Clinicopathological features and outcomes of T1 CRC

We assessed demographic and clinical characteristics (tumor location, tumor size, gross type, histologic type, SM invasion depth, vertical margin, lymphatic invasion,

venous invasion, and budding grade) and long-term outcomes of pedunculated-type T1 CRCs after endoscopic or surgical resection. All pathological slides of the tumors were reassessed by an experienced gastrointestinal pathologist (F.S.) who was blinded to the clinical outcomes. The incidence of LN metastasis of surgically treated lesions was analyzed. Physical examination, chest radiography, computed tomography (CT) of the abdomen and pelvis, and blood tests including carcinoembryonic antigen level were performed every 6 months postoperatively for the first 3 years and every 12 months thereafter and a total colonoscopy was performed every year, in principle. Recurrence was recorded as local, distant, and overall recurrence. Recurrent lesions were identified by colonoscopy, CT, or transabdominal ultrasound. Local recurrence after surgical resection was defined as recurrence within the surgical field for T1 CRC or within the pelvis for T1 rectal carcinoma.

Statistical analysis

Values are reported as means (with standard deviations). Fisher's exact test was used to compare categorical variables. Analyses were performed with JMP Statistical software, version 9.02 (SAS Institute, Cary, NC, USA). p values <0.05 were considered statistically significant. There was no adjustment of nominal p values to correct for multiple testing of outcome data arising from individual patients, because the main focus of this research was exploratory in nature. Disease-free survival and overall survival rates were calculated by the Kaplan–Meier method.

Results

The demographics and clinical characteristics of pedunculated-type T1 CRC cases are shown in Table 1. The treatment method was ER alone in 95 cases (54 %), additional surgery after ER in 66 (38 %), and surgical resection alone in 15 (8 %). Initial ER was performed in 161 (91 %) cases and the histological en bloc resection rate was 96 % (154/161). The rates of post-ER bleeding and perforation were 2 (3/161) and 0 % (0/161), respectively (Table 2). Most tumors [173 (98 %)] were well- or moderately differentiated adenocarcinomas, but three (2 %) were poorly differentiated adenocarcinomas. Mean tumor size was 17.5 ± 3.5 (range, 6–75) mm, with 137 (78 %) located in the left colon, 21 (12 %) in the right colon, and 18 (10 %) in the rectum. SM invasion <1000 μm was observed in 100 cases, with head invasion in 78 (44 %) and stalk invasion in 19 (11 %) while invasion >1000 μm was observed in 76 cases, with stalk invasion in 50 (28 %).

Table 1 Clinicopathological features of pedunculated-type T1 CRC

Variables	Total (n = 176)	ER alone (n = 95)	Additional surgery after ER (n = 66)	Surgical resection (n = 15)
Age (years), mean (range)	64.2 (29–84)	64.8 (32–84)	63.5 (29–82)	64.1 (43–77)
Sex (M/F), n (%)	138 (78)/38 (22)	77 (81)/18 (19)	50 (76)/16 (24)	11 (73)/4 (27)
Location, n (%)				
Right colon	21 (12)	16 (17) ^a	4 (6) ^b	1 (7)
Left colon	137 (78)	67 (71) ^c	57 (86) ^d	13 (87)
Rectum	18 (10)	12 (12)	5 (8)	1 (6)
Tumor size (mm)				
Mean (range)	17.5 (6–75)	18.1 (6–75) ^e	19 (6–50) ^f	26.9 (13–50) ^g
Histologic type				
Tub/pap	173 (98)	94 (99)	64 (97)	15 (100)
Por/sig/muc	3 (2)	1 (1)	2 (3)	0 (0)
SM depth (μm), n (%)				
<1000	100 (57)	70 (74) ^h	26 (39) ⁱ	4 (27) ^j
With head invasion	78 (44)	53 (56)	22 (33)	3 (20)
≥1000	76 (43)	25 (26) ^h	40 (61) ⁱ	11 (73) ^j
Vertical margin positive	2 (1)	2 (2)	0 (0)	0 (0)
Lymphatic invasion positive	38 (22)	10 (11) ^k	24 (36) ^l	4 (27)
Venous invasion positive	14 (8)	4 (4) ^m	9 (14) ⁿ	1 (7) ^o
Budding grade 2/3	24 (14)	9 (9) ^p	14 (21) ^q	1 (7)
E-curable/non-e-curable, n (%)	82 (47)/94 (53)	61 (64)/34 (36) ^r	18 (27)/48 (73) ^s	3 (20)/12 (80) ^t

Patients who met the curative criteria for T1 CRC after ER as stated in the JSCCR guidelines were defined as “e-curable”, while those who did not meet the criteria were defined as “non-e-curable”

ER endoscopic resection, muc mucinous adenocarcinoma, pap papillary adenocarcinoma, por poorly differentiated adenocarcinoma, sig signet-ring cell carcinoma, tub tubular adenocarcinoma, SM submucosal

a vs. b, c vs. d, e vs. g, f vs. g, h vs. i, h vs. j, k vs. l, m vs. n, m vs. o, p vs. q, r vs. s, r vs. t: $p < 0.05$

There were 38 cases of lymphatic invasion (22 %), 14 of venous invasion (8 %), and 24 of budding grade 2/3 (14 %) (Table 1). Among T1 CRCs with invasion above Haggitt’s line ($n = 107$), the rates of SM invasion depth ≥ 1000 μm and venous invasion were 24 (26/107) and 5 % (5/107), respectively, compared with 72 (50/69) and 13 % (9/69) of T1 CRCs that had invaded beyond Haggitt’s line ($n = 69$) ($p < 0.05$). The rate of lymphatic invasion of T1 CRCs with histological invasion above Haggitt’s line was 17 % (18/107), compared with 29 % (20/69) of T1 CRC that had invaded beyond Haggitt’s line ($p = 0.06$). A total of 82

patients (47 %) met the JSCCR curative criteria. The overall incidence of LN metastasis was 5 % [4/81; 95 % confidence interval (CI) 1.4–12 %; three cases of SM invasion depth ≥ 1000 μm (stalk invasion) and lymphatic invasion, one case of head invasion and budding grade 2/3] (Table 3). The incidence of LN metastasis of e-curable and non-e-curable lesions was 0 % (0/21; 95 % CI 0–13 %) and 7 % (4/60; 95 % CI 1.8–16.2 %), respectively. There was no local or metastatic recurrence in any of the e-curable patients, but six of them died of another cause: three, another organ carcinoma; one, myocardial infarction; one, cerebral hemorrhage; one, decrepitude; average observation period of 80 months. There was no local recurrence in the non-e-curable patients; however, distant metastasis was observed in one patient [2 %; well-differentiated adenocarcinoma, SM invasion depth ≥ 1000 μm (stalk invasion), budding grade 1, ly1, v0, HM0, VM0], with carcinoma recurring in the liver and lung 7 and 36 months after additional surgery, respectively (Table 3). Death due to primary disease was not observed in non-e-curable patients at the latest follow-up, but six of them died of another cause (three of another organ carcinoma, two of myocardial

Table 2 Clinical outcomes of endoscopic resection for pedunculated-type T1 CRC

En bloc resection rate	96 % (154/161)
Histological en bloc resection rate	96 % (154/161)
Horizontal margin positive, n (%)	1 % (2/161)
Vertical margin positive, n (%)	0 % (0/161)
Adverse event	
Delayed bleeding	2 % (3/161)
Perforation	0 % (0/161)

Table 3 Clinicopathological features of pedunculated-type T1 CRC with lymph node metastasis

No. of cases	Sex	Age	Location	Tumor size (mm)	Histologic grade	Submucosal depth (µm)	Vascular invasion	Budding grade	Vertical margin	Residual tumor	Recurrence site	Time to recurrence (months)	Alive/dead
Additional surgery after ER													
1	Male	66	Sigmoid	20	Well	1500	ly1 v0	G1	(-)	(-)	Liver • lung	7	Alive
Surgical resection alone													
2	Male	48	Sigmoid	35	Well	1500	ly1 v0	G1	(-)	(-)			Alive
3	Male	66	Sigmoid	20	Well	6000	ly1 v0	G1	(-)	(-)			Alive
4	Male	71	Sigmoid	20	Well	Head invasion	ly0 v0	G2	(-)	(-)			Alive

Well well-differentiated adenocarcinoma

infarction, and one of decrepitude; average observation period of 72 months). As shown in Fig. 1, a very low incidence of recurrence was observed in patients with pedunculated-type CRC. The corresponding overall survival rates of the e-curable patients were 94.7, 100, and 100 % in the ER group, ER plus surgical resection group, and surgical resection group, respectively, while the corresponding overall survival rates of the non-e-curable patients were 90.9, 100, and 100 % (Fig. 2). None of the patients had adverse events after ER or postoperative adverse events requiring emergency surgery, including perforation or bleeding, and no mortality occurred at the time of surgical resection after ER.

Discussion

This is the first multicenter retrospective cohort study that assessed the clinical validity of the JSCCR guidelines based on long-term outcomes of pedunculated-type T1 CRCs after ER or surgical resection. The results of this study support the validity of the JSCCR curative criteria for pedunculated-type T1 CRCs after ER because e-curable patients showed no increased risk for recurrence and had good outcomes. Previously, histopathological factors such as deep SM invasion, poor differentiation, angiolymphatic invasion, presence of a poorly differentiated area and muconodules at the site of deepest invasion, and budding grade were reported to be associated with LN metastasis in T1 CRC [7, 14, 19, 26]. A few studies showed that SM depth was not significantly related to LN metastasis in patients with T1 CRC [8, 21, 24, 27, 28]. We previously reported an incidence of LN metastasis of only 1.2 % (95 % CI, 0.25–3.48 %) in T1 CRC without three of the four risk factors (i.e., all except SM invasion depth <1000 µm) for LN metastasis according to the JSCCR guidelines [8]. Measurement of the depth of SM invasion is relatively simple in cases of sessile-type T1 CRC [19]; however, it is relatively complicated in pedunculated-type T1 CRC due to the presence of stalks, the varying length of these stalks and tangled muscularis mucosae.

Since Haggitt et al. [20] proposed a classification of the level of invasion of CRC arising from polyps in 1985, the classification of SM invasion has been widely used in pathological evaluation. Although this classification is very simple, the 129 analyzed cases consisted of both non-pedunculated and pedunculated-type T1 CRCs, with only 70 cases of pedunculated-type T1 CRC [20]. Therefore, the use of Haggitt’s classification tends to lead to over-treatment of cases without LN metastasis and it does not consider recently identified risk factors such as tumor budding [7]. In a retrospective multicenter study involving 384

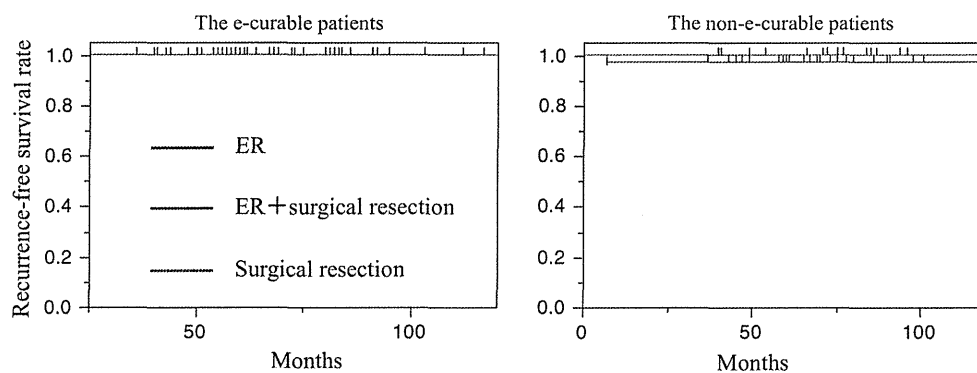


Fig. 1 Kaplan–Meier curves of disease-free survival of patients with pedunculated-type T1 colorectal carcinoma. Disease-free survival (DFS) rates in the e-curable patients were all 100 %, regardless of treatment with endoscopic resection (ER) alone, ER plus additional surgical resection, or surgical resection alone. Disease-free survival

rates were 100, 97.2, and 100 % in the non-e-curable patients treated with endoscopic resection (ER) alone, ER plus additional surgical resection, and surgical resection alone, respectively, with no significant differences between the groups ($p = 0.74$)

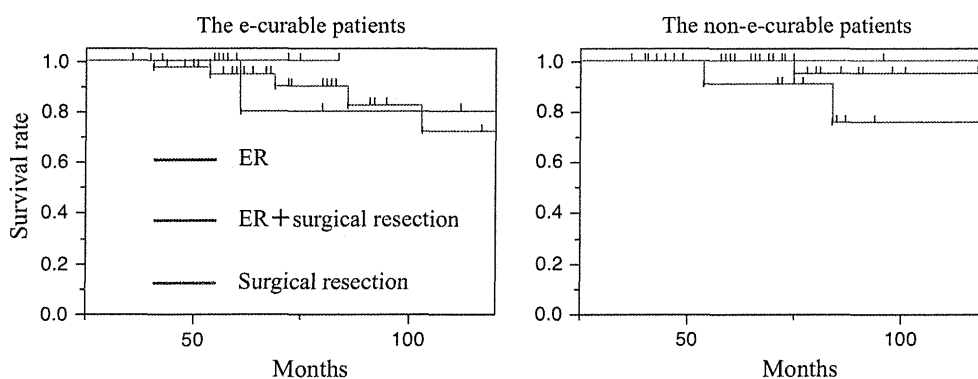


Fig. 2 Kaplan–Meier curves of overall survival of the non-e-curable patients. Overall survival (OS) rates of the e-curable patients treated with ER alone, ER plus additional surgical resection, and surgical resection alone were 94.7, 100, and 100 %, respectively, with no significant differences between the groups ($p = 0.81$). OS rates of the

non-e-curable patients treated with ER alone, ER plus additional surgical resection, and surgical resection alone were 90.9, 100, and 100 %, respectively, with no significant differences between the groups ($p = 0.10$)

pedunculated-type T1 CRC patients treated with ER or surgical resection, Matsuda et al. [15] reported that the incidence of LN metastasis of pedunculated-type T1 CRC was 0 % (0/101) with invasion above Haggitt's line and 6.2 % (8/129) with invasion beyond Haggitt's line, and they suggested that pedunculated-type T1 CRC with invasion above Haggitt's line could be managed by ER alone. However, the follow-up period of their study was short, and there was a lack of data on tumor budding, which has been identified as an important risk factor for LN metastasis.

A meta-analysis revealed that lymphatic vessel invasion identified by an anti-human podoplanin antibody and tumor budding were significantly associated with T1 CRC LN metastasis [29]. Several studies with a small number of analyzed cases have reported the rate of LN metastasis of pedunculated-type T1 CRCs with invasion above Haggitt's line (Table 4) [10, 12, 15, 30–32]. In

Collacchio's series, the incidence of LN metastasis of T1 CRCs with invasion above Haggitt's line was 29 % (5/17). The five patients with LN metastasis belonged to their case series in which two had documented carcinoma within the lymphatics of the polyp and one had an invasive anaplastic carcinoma [31]. Fenoglio et al. reported two pedunculated-type T1 CRCs with LN metastasis in which carcinomatous invasion was above Haggitt's line and that both cases had lymphatic invasion [33]. Kitajima et al. [14] reported that LN metastasis was observed in three cases with invasion above Haggitt's line and a prediction of the absence of LN metastasis based on SM depth alone was considered difficult. All three cases with invasion above Haggitt's line and LN metastasis were positive for lymphatic invasion. In the present study, the overall incidence of LN metastasis was 5 % (4/81). Our results showed that one of four cases with LN metastasis had "head invasion". Therefore, ER cannot be

Table 4 Literature series about outcomes of pedunculated-type T1 CRC

Author	Published year	No. of patients	No. of surgical resection	Rate of residual tumor	Rate of LN metastasis	Rate of LN metastasis		Recurrence rate
						Deepest portion of carcinoma invasion		
						Within Haggitt's line ^a	Beyond Haggitt's line ^a	
Wolff/Shinya	1975	33	11	27 % (3/11)	0 % (0/11)	–	–	–
Shantney	1976	28	23	–	4 % (1/23)	0 % (0/14)	1 % (1/9)	0 % (0/28)
Nivatvongs	1978	16	3	0 % (0/3)	33 % (1/3)	0 % (0/2)	100 % (1/1)	0 % (0/16)
Colacchio	1981	39	24	0 % (0/24)	25 % (6/24)	29 % (5/17)	14 % (1/7)	–
Kodaira	1981	41	41	–	4.9 % (2/41)	–	–	–
Cooper	1983	49	29	–	14 % (4/29)	0 % (0/26)	17 % (4/23)	2 % (1/49)
Pines	1990	43	19	0 % (0/19)	0 % (0/19)	0 % (0/11)	0 % (0/8)	0 % (0/43)
Kikuchi	1995	23	3	–	0 % (0/3)	–	–	–
Kitajima	2004	141	141	–	7.1 % (10/141)	–	–	–
Matsuda	2011	384	230	0 % (0/230)	3.5 % (8/230)	0 % (0/101)	6.2 % (8/129)	0.3 % (1/340)
Kobayashi	2012	20	20	–	5 % (1/20)	–	–	5 % (1/20)
Our series	2015	176	81	0 % (0/81)	4.9 % (4/81)	2.4 % (1/41)	7.5 % (3/40)	0.8 % (1/116)

LN lymph node

^a Haggitt's line: The line of Haggitt's level 2

considered curative for pedunculated-type T1 CRC with head invasion alone, as defined in the JSCCR guidelines.

The JSCCR criteria were established based on an analysis of histologic data of T1 CRC in surgically resected specimens [14], and there have been few reports on surveillance data after ER for T1 CRC [13, 21–23, 34]. Recurrence in patients with T1 CRC after surgical curative resection has also been reported [6, 16]. As yet, the characteristics and types of recurrence remain unclear. In this study, a very low incidence of recurrence was observed in patients with pedunculated-type CRC. It is possible that no significance was seen in disease-free survival rates because additional surgery restrained the local or LN recurrence of carcinomas in non-e-curable patients. However, distant metastasis was observed in one patient with carcinoma recurring in the liver and lung 7 and 36 months after additional surgery with LN dissection.

The overall survival rates was low only in the ER, although overall survival rates showed no significance in the non-e-curable patients treated with ER alone, ER plus additional surgical resection, and surgical resection alone, respectively. This finding is attributable to the fact that patients treated with ER alone included non-e-curable patients who could not undergo surgery because of anesthesia concerns and/or advanced age.

Our study revealed that 161 (91 %) pedunculated-type T1 CRC cases received ER as the initial treatment; histological en bloc resection rate was 96 % (154/161); the rate

of adverse events was extremely low; and there were no local recurrence cases. These results suggested pedunculated-type T1 CRCs could be managed by polypectomy/EMR alone when en bloc resection is possible.

Endoscopic submucosal dissection (ESD) is regarded as a reliable method for en bloc resection regardless of tumor size and a possible standard technique for total excisional biopsy for clinical T1 CRC after an accurate preoperative diagnosis and precise histopathological diagnosis are reached [3]. ESD is an effective procedure for removal of large pedunculated-type CRC when it is difficult to correctly position the snare over the stalk for en bloc resection [35]. The JSCCR guidelines clearly state that additional treatment should be performed only after systematically evaluating the predicted curability based on various LN metastasis risk factors and the patient's background (e.g., age, concomitant disease, operative method, patient's wishes, life expectancy, and performance status) and after obtaining informed consent from the patient [19]. The findings of the present study demonstrated that we should follow the JSCCR guidelines after treatment for pedunculated-type T1 CRC.

This study has some limitations. First, this study was a multicenter retrospective cohort study based on clinical records. Second, this study might be affected by selection bias because it was not randomized. Third, we reevaluated the pathological diagnosis and features including tumor budding; however, we did not reevaluate lymphovascular

invasion using immunohistochemical staining for all cases. Routine use of immunohistochemistry should be considered in future retrospective studies. Fourth, the statistical power was not sufficient to discern small differences in the group analysis of more comprehensive pathologic factors. Large-scale multicenter prospective investigations are needed to evaluate the long-term outcomes of T1 CRC in the near future.

In conclusion, our data support the validity of the JSCCR curative criteria (well/moderately differentiated or papillary carcinoma, no vascular invasion, SM invasion depth <1000 μ m, and budding grade 1) for pedunculated-type T1 CRCs after ER. ER cannot be considered curative for pedunculated-type T1 CRC with head invasion alone. Additional surgery after ER should be considered only after taking into account the patient's condition and the concrete risk of LN metastasis in each case.

Compliance with ethical standards

Conflict of interest The authors declare that they have no conflicts of interest.

References

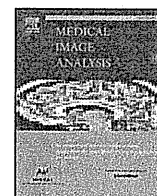
- Muto T, Oya M. Recent advances in diagnosis and treatment of colorectal T1 carcinoma. *Dis Colon Rectum*. 2003;46:S89–93.
- Kyzer S, Begin LR, Gordon PH, et al. The care of patients with colorectal polyps that contain invasive adenocarcinoma: endoscopic polypectomy or colectomy? *Cancer*. 1992;70:2044–50.
- Asayama N, Oka S, Tanaka S, et al. Endoscopic submucosal dissection as total excisional biopsy for clinical T1 colorectal carcinoma. *Digestion*. 2015;27:216–22.
- Tanaka S, Yokota T, Saito D, et al. Clinicopathologic features of early rectal carcinoma and indications for endoscopic treatment. *Dis Colon Rectum*. 1995;38:959–63.
- Tanaka S, Haruma K, Teixeira CR, et al. Endoscopic treatment of submucosal invasive colorectal carcinoma with special reference to risk factors for lymph node metastasis. *J Gastroenterol*. 1995;30:710–7.
- Kobayashi H, Mochizuki H, Morita T, et al. Characteristics of recurrence after curative resection for T1 colorectal cancer: Japanese multicenter study. *J Gastroenterol*. 2011;46:203–11.
- Ueno H, Mochizuki H, Hashiguchi Y, et al. Risk factors for an adverse outcome in early invasive colorectal carcinoma. *Gastroenterology*. 2004;127:385–94.
- Nakadoi K, Tanaka S, Kanao H, et al. Management of T1 colorectal carcinoma with special reference to criteria for curative endoscopic resection. *J Gastroenterol Hepatol*. 2012;27:1057–62.
- Shatney CH, Lober PH, Gilbertson V, et al. Management of focally malignant pedunculated adenomatous colorectal polyps. *Dis Colon Rectum*. 1976;19:334–41.
- Wolff WI, Shinya H. Definitive treatment of “malignant” polyps of the colon. *Ann Surg*. 1975;182:516–25.
- Kodaira S, Teramoto T, Ono S, et al. Lymph node metastases from carcinomas developing in pedunculated and semipedunculated colorectal adenomas. *Aust N Z J Surg*. 1981;51:429–33.
- Pines A, Bat L, Shemesh E, et al. Invasive colorectal adenomas: surgery versus colonoscopic polypectomy. *J Surg Oncol*. 1990;43:53–5.
- Kikuchi R, Takano M, Takagi K, et al. Management of early invasive colorectal cancer. Risk of recurrence and clinical guidelines. *Dis Colon Rectum*. 1995;38:1286–95.
- Kitajima K, Fujimori T, Fujii S, et al. Correlations between lymph node metastasis and depth of submucosal invasion in submucosal invasive colorectal carcinoma: a Japanese collaborative study. *J Gastroenterol*. 2004;39:534–43.
- Matsuda T, Fukuzawa M, Uraoka T, et al. Risk of lymph node metastasis in patients with pedunculated type early invasive colorectal cancer: a retrospective multicenter study. *Cancer Sci*. 2011;102:1693–7.
- Kobayashi H, Higuchi T, Uetake H, et al. Resection with en bloc removal of regional lymph node after endoscopic resection for T1 colorectal cancer. *Ann Surg Oncol*. 2012;19:4161–7.
- Gordon MS, Cohen AM. Management of invasive carcinoma in pedunculated colorectal polyps. *Oncology*. 1989;3:99–104.
- Colacchio TA, Forde KA, Scantlebury VP. Endoscopic polypectomy: inadequate treatment for invasive colorectal carcinoma. *Ann Surg*. 1981;194:704–7.
- Watanabe T, Itabashi M, Shimada Y, et al. Japanese Society for Cancer of the Colon and Rectum (JSCCR) Guidelines 2014 for treatment of colorectal cancer. *Int J Clin Oncol*. 2015;20:207–39.
- Haggitt RC, Glotzbach RE, Soffer EE, et al. Prognostic factors in colorectal carcinomas arising in adenomas: implications for lesions removed by endoscopic polypectomy. *Gastroenterology*. 1985;89:328–36.
- Yoshii S, Nojima M, Noshio K, et al. Factors associated with risk for colorectal cancer recurrence after endoscopic resection of T1 tumors. *Clin Gastroenterol Hepatol*. 2014;2:292–302.
- Ikematsu H, Yoda Y, Matsuda T, et al. Long-term outcomes after resection for submucosal invasive colorectal cancers. *Gastroenterology*. 2014;144:551–9.
- Yoda Y, Ikematsu H, Matsuda T, et al. A large-scale multicenter study of long-term outcomes after endoscopic resection for submucosal invasive colorectal cancer. *Endoscopy*. 2013;45:718–24.
- Choi DH, Sohn DK, Chang HJ, et al. Indications for subsequent surgery after endoscopic resection of submucosally invasive colorectal carcinomas: a prospective cohort study. *Dis Colon Rectum*. 2009;52:438–45.
- Di Gregorio C, Bonetti LR, de Gaetani C, et al. Clinical outcome of low- and high-risk malignant colorectal polyps: results of a population-based study and meta-analysis of the available literature. *Intern Emerg Med*. 2014;9:151–60.
- Tanaka S, Haruma K, Oh-e H, et al. Conditions of curability after endoscopic resection for colorectal carcinoma with submucosally massive invasion. *Oncol Rep*. 2000;7:783–8.
- Okabe S, Shia J, Nash G, et al. Lymph node metastasis in T1 adenocarcinoma of the colon and rectum. *J Gastrointest Surg*. 2004;8:1032–9.
- Tateishi Y, Nakanishi Y, Taniguchi H, et al. Pathological prognostic factors predicting lymph node metastasis in submucosal invasive (T1) colorectal carcinoma. *Mod Pathol*. 2010;23:1068–72.
- Wada H, Shiozawa M, Katayama K, et al. Systematic review and meta-analysis of histopathological predictive factors for lymph node metastasis in T1 colorectal cancer. *J Gastroenterol*. 2015;50:727–34.
- Nivatvongs S, Goldberg SM. Management of patients who have polyps containing invasive carcinoma removed via colonoscope. *Dis Colon Rectum*. 1978;21:8–11.
- Colacchio TA, Forde KA, Scantlebury VP. Endoscopic polypectomy: inadequate treatment for invasive colorectal carcinoma. *Ann Surg*. 1981;194:704–7.
- Cooper HS. Surgical pathology of endoscopically removed malignant polyps of the colon and rectum. *Am J Surg Pathol*. 1983;7:613–23.

33. Fenoglio CM, Kaye GI, Lane N. Distribution of human colonic lymphatics in normal, hyperplastic, and adenomatous tissue. Its relationship to metastasis from small carcinomas in pedunculated adenomas, with two case reports. *Gastroenterology*. 1973;64:51–66.
34. Oka S, Tanaka S, Kanao H, et al. Mid-term prognosis after endoscopic resection for submucosal colorectal carcinoma: summary of a multicenter questionnaire survey conducted by the colorectal endoscopic resection standardization implementation working group in Japanese Society for Cancer of the Colon and Rectum. *Dig Endosc*. 2011;23:190–4.
35. Choi YS, Lee JB, Lee EJ, et al. Can endoscopic submucosal dissection technique be an alternative treatment option for a difficult giant (≥ 30 mm) pedunculated colorectal polyp? *Dis Colon Rectum*. 2013;56:660–6.



Contents lists available at ScienceDirect

Medical Image Analysis

journal homepage: www.elsevier.com/locate/media

Local fractal dimension based approaches for colonic polyp classification



Michael Häfner^a, Toru Tamaki^b, Shinji Tanaka^c, Andreas Uhl^d, Georg Wimmer^{d,*},
Shigeto Yoshida^c

^a St. Elisabeth Hospital, Landstraßer Hauptstraße 4a, Vienna A-1030, Austria

^b Department of Information Engineering, Graduate School of Engineering, Hiroshima University, 1-4-1 Kagamiyama, Higashi-hiroshima, Hiroshima 739-8527, Japan

^c Department of Endoscopy, Hiroshima University Hospital, 1-2-3 Kasumi, Minami-ku, Hiroshima 734-8551, Japan

^d Department of Computer Sciences, Jakob Haringerstrasse 2, University of Salzburg, Salzburg 5020, Austria

ARTICLE INFO

Article history:

Received 24 October 2014

Revised 10 July 2015

Accepted 20 August 2015

Available online 29 August 2015

Keywords:

Polyp classification

Local fractal dimension

Texture recognition

Viewpoint invariance

ABSTRACT

This work introduces texture analysis methods that are based on computing the local fractal dimension (LFD; or also called the local density function) and applies them for colonic polyp classification. The methods are tested on 8 HD-endoscopic image databases, where each database is acquired using different imaging modalities (Pentax's i-Scan technology combined with or without staining the mucosa) and on a zoom-endoscopic image database using narrow band imaging. In this paper, we present three novel extensions to a LFD based approach. These extensions additionally extract shape and/or gradient information of the image to enhance the discriminativity of the original approach. To compare the results of the LFD based approaches with the results of other approaches, five state of the art approaches for colonic polyp classification are applied to the employed databases. Experiments show that LFD based approaches are well suited for colonic polyp classification, especially the three proposed extensions. The three proposed extensions are the best performing methods or at least among the best performing methods for each of the employed databases.

The methods are additionally tested by means of a public texture image database, the UIUCTex database. With this database, the viewpoint invariance of the methods is assessed, an important feature for the employed endoscopic image databases. Results imply that most of the LFD based methods are more viewpoint invariant than the other methods. However, the shape, size and orientation adapted LFD approaches (which are especially designed to enhance the viewpoint invariance) are in general not more viewpoint invariant than the other LFD based approaches.

© 2015 Elsevier B.V. All rights reserved.

1. Introduction

In this paper, texture analysis methods are applied for the automated classification of colonic polyps in endoscopic images under unknown viewpoint and illumination conditions. Endoscopic images occur with different scales, orientations or perspectives, depending on the distance and perspective of the camera to the object. Fig. 1 shows some examples for the field of view depending on the endoscopic viewpoint to the mucosal wall.

The varying viewpoint condition combined with the large intra-class and small inter-class variations of polyps make it very difficult to distinguish between different types of polyps. The viewpoint invariance of the employed methods is an important feature to at least reduce the problem with the varying viewpoint conditions.

Uhl et al. (2011) and Häfner et al. (2014c) showed that methods based on fractal analysis are able to combine viewpoint invariance with high discriminativity and are quite suitable for endoscopic image classification.

The term "fractal" was first used by the mathematician Benoit Mandelbrot as an indication of objects whose complex geometry cannot be characterized by an integral dimension. Fractal geometry is able to describe the irregular or fragmented shape of natural features as well as other complex objects that traditional Euclidean geometry fails to analyze. The fractal dimension is the key quantity to describe the fractal geometry and the heterogeneity of irregular shapes. Roughly spoken, the fractal dimension is a ratio that compares how the detail of a shape changes with the scale at which it is measured.

However, the fractal dimension is only one number, which is not enough to describe an object.

As an extension to the classical fractal analysis, multifractal analysis provides more powerful descriptions. Applied to image processing, first define a point characterization on an image according to

* Corresponding author.

E-mail addresses: uhl@cosy.sbg.ac.at (A. Uhl), gwimmer@cosy.sbg.ac.at (G. Wimmer).

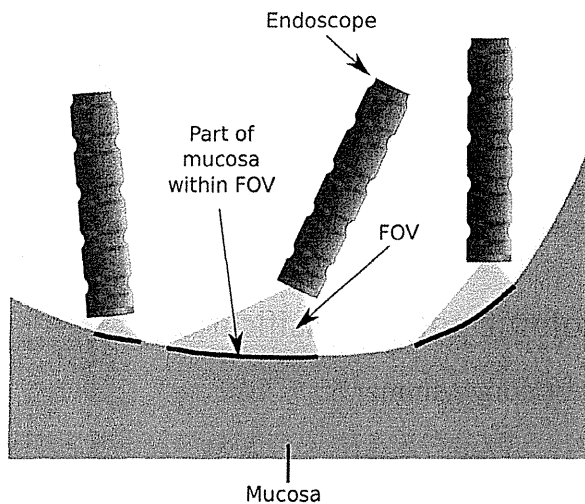


Fig. 1. The field of view (FOV) depending on the endoscopic viewpoint to the mucosal wall.

some criteria (e.g., the intensity values of the pixels), then the fractal dimensions are computed for every point set from this categorization (e.g., categorize the image pixels by their intensity and obtain binary images by setting a pixel to 0 if its intensity value is in the considered set and to 1 otherwise). The collection of the fractal dimensions of the binary images is called a multi fractal spectrum (MFS) vector.

Another extension to the classical analysis to provide a more powerful description is to compute local fractal features. These features are already the norm in fractal based image segmentation (Chaudhuri and Sarkar, 1995; Xia et al., 2006).

In Xu et al. (2009), local fractal based features (we denote them as local fractal dimensions, LFD's) are computed densely followed by applying multifractal analysis to these features (categorize the LFD's by their values, thereby obtain binary images followed by computing the fractal dimension of the binary images). Another approach (Varma and Garg, 2007) using the LFD is pre-filtering the image with the MR8 filter bank obtaining eight filtered images on which the LFD's are computed. Subsequently, the bag of visual words (BoW) approach is used to build histograms of the LFD's. It has been shown that the LFD is invariant to bi-Lipschitz transformations, such as local affine or perspective transformations and certain smooth, non-linear transformations (Xu et al., 2009). The LFD is also invariant to local affine illumination changes as showed in Xu et al. (2009).

Roughly speaking, the LFD at an arbitrary location of an image is computed by summing up intensity values in disk shaped areas with fixed radii surrounding the considered (pixel) location followed by analyzing the increase of the sums for increasing radii. Actually, the scale and perspective of the object or texture in the image at the considered location is not taken into account, the radii are always the same and the areas are always disk shaped. In Häfner et al. (2014c), a more viewpoint adaptive approach is presented. This LFD based approach uses ellipsoidal areas instead of disk shaped areas. The sizes, shapes and orientations of the ellipsoidal areas are adapted to the local texture structure by analyzing the shape, size and orientation of connected components (blobs). Instead of a dense computation of the LFD's like in Xu et al. (2009) and Varma and Garg (2007), the size, shape and orientation adapted LFD's in Häfner et al. (2014c) are computed only for interest points, more precisely only for those points that are the centers of the area of a blob.

A review about methods using fractal and multifractal analysis is presented in Lopes and Betrouni (2009).

In this work we compare methods based on the LFD, compare their classification results on different image databases, analyze the reasons for those results and examine the affine invariance of the

methods. We will test the LFD approaches on nine different endoscopic image databases, which consist of highly detailed endoscopic images with nine different imaging modalities. Additionally we apply the LFD based approaches on a public texture database with huge viewpoint variations, the UIUCTex database (Lazebnik et al., 2005).

The contributions of this manuscript are as follows:

- We apply seven LFD based methods for the automated classification of colonic polyps using nine different endoscopic image databases. Eight databases are gathered using an HD-endoscope with eight different imaging modalities (Pentax's i-Scan in combination with staining the mucosa) and one database is gathered using a zoom-endoscope with narrow band imaging (NBI) as imaging modality. To the best of our knowledge, this is the highest number of endoscopic polyp databases that has been used in publications so far. The results of the LFD based methods are compared and the differences between the methods and their impacts to the results are analyzed.
- Five (non LFD based) state-of-the-art approaches for colonic polyp classification are applied to the classification of our databases to compare their results with the results of the LFD based methods.
- We present three novel extensions of an LFD approach. For each database, the results of these extensions are among the best results of all the employed methods.
- We assess the viewpoint invariance of the methods by means of a public texture database, the UIUCTex database (Lazebnik et al., 2005). Results imply, that most of the LFD based methods are more viewpoint invariant than the other methods. The size, shape and orientation adapted LFD methods are generally not more viewpoint invariant than the other LFD based methods.

Already in Häfner et al. (2014c), an LFD-based method was proposed for the classification of colonic polyps. However, this publication used only one endoscopic image database (one of our 8 HD-endoscopic image databases) and compared the result of the proposed method with only one other LFD based approach and three non LFD based approaches. Furthermore, neither the differences between the two LFD based approaches were analyzed nor the viewpoint invariance of the approaches was tested.

This paper is organized as follows. In Section 2 we briefly introduce the concept of the computer-assisted diagnosis of polyps by the automated classification of mucosa texture patches and review the corresponding state-of-the-art. In Section 3, we describe the feature extraction approaches and compare the approaches that are based on computing the LFD. The experimental setup, the used databases and the results are presented in Section 4. Section 5 presents the discussion and Section 6 concludes our work. The acronyms used in this work are listed in the Appendix.

2. Colonic polyp classification

Colonic polyps have a rather high prevalence and are known to either develop into cancer or to be precursors of colon cancer. Hence, an early assessment of the malignant potential of such polyps is important as this can lower the mortality rate drastically. As a consequence, a regular colon examination is recommended, especially for people at an age of 50 years and older. The current gold standard for the examination of the colon is colonoscopy, performed by using a colonoscope. Modern endoscopy devices are able to take pictures or videos from inside the colon, allowing to obtain images (or videos) for a computer-assisted analysis with the goal of detecting and diagnosing abnormalities.

Colonic polyps are a frequent finding and are usually divided into hyperplastic, adenomatous and malignant. In order to determine a diagnosis based on the visual appearance of colonic polyps, the pit pattern classification scheme was proposed by Kudo et al. (1994). A pit pattern refers to the shape of a pit, the opening of a colorectal crypt.

This classification scheme allows to differentiate between normal mucosa and hyperplastic lesions, adenomas (a pre-malignant condition), and malignant cancer based on the visual pattern of the mucosal surface. The removal of hyperplastic polyps is unnecessary and the removal of malignant polyps maybe hazardous. Thus, this classification scheme is useful to decide which lesions need not, which should, and which most likely cannot be removed endoscopically. For these reasons, assessing the malignant potential of lesions at the time of colonoscopy is important, as this would allow to perform targeted biopsy.

The various pit pattern types are presented in Fig. 3e and f. The pit pattern classification scheme differentiates between six types. Types I (normal mucosa) and II (hyperplastic polyps) are characteristics of non-neoplastic lesions, type III-S, III-L and IV are typical for adenomatous polyps and type V is strongly suggestive to malignant cancer.

To enable an easier detection and diagnosis of the extent of a lesion, there are two common image enhancement technologies:

1. Conventional chromoendoscopy (CC) came into clinical use 40 years ago. By staining the mucosa using (indigocarmine) dye spray, it is easier to find and classify polyps.
2. Digital chromoendoscopy is a technique to facilitate “chromoendoscopy without dyes” (Kiesslich, 2009). The strategies followed by major manufacturers differ in this area:
 - In narrow band imaging (NBI, Olympus), narrow bandpass filters are placed in front of a conventional white-light source to enhance the detail of certain aspects of the surface of the mucosa.
 - The i-Scan (Pentax) image processing technology (Kodashima and Fujishiro, 2010) is a digital contrast method which consists of combinations of surface enhancement, contrast enhancement and tone enhancement. The FICE system (Fujinon) decomposes images by wavelength and then directly reconstructs images with enhanced mucosal surface contrast. Both systems (i-Scan and FICE) apply post-processing to the reflected light and thus are called “computed virtual chromoendoscopy (CVC)”.

Previous works for the computer assisted staging of colon polyps, which are using endoscopes producing highly detailed images in combination with different imaging modalities, can be divided in three categories: high definition (HD) endoscope combined with or without staining the mucosa and the i-Scan technology (Häfner et al., 2014c), high-magnification chromoendoscopy (Häfner et al., 2009) and high-magnification endoscopy combined with NBI (Gross et al., 2012; Tamaki et al., 2013). In this work we use highly detailed images acquired by an HD endoscope without magnification in combination with CC and CVC (the i-Scan technology) and images acquired by a high-magnification endoscope combined with NBI.

Further examples of approaches for colonic polyp classification are Iakovidis et al. (2005), Karkanis et al. (2003), Maroulis et al. (2003), and Iakovidis et al. (2006).

In addition to classical endoscopy, endomicroscopy and wireless capsule endoscopy are used for the examination of the gastrointestinal tract. Endomicroscopy (Jabbour et al., 2012) is a technique to obtain histology-like images and is also known as ‘optical biopsy’. For example André et al. (2011, 2012) show state of the art approaches based on semantics and visual concepts for the automated diagnosis of colonic polyps using endomicroscopy.

Wireless capsule endoscopy (Iakovidis and Koulaouzidis, 2015; Yuce and Dissanayake, 2012) is mainly used to examine parts of the gastrointestinal tract that cannot be seen with other types of endoscopes. The capsule has the size and shape of a pill and contains a tiny camera. After a patient swallows the capsule, it takes images of the inside of the gastro-intestinal tract. An example for the automated

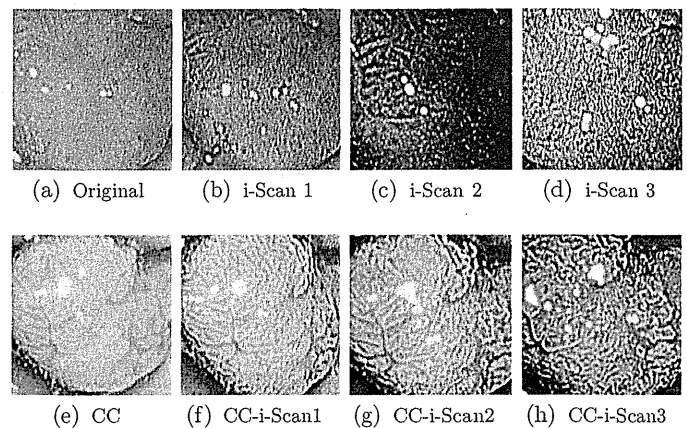


Fig. 2. Images of a polyp using digital (i-Scan) and/or conventional chromoendoscopy (CC).

detection and classification of colonic polyps using capsule endoscopy can be seen in Romain et al. (2013).

2.1. HD endoscopy in combination with the i-Scan image processing technology

In this work, the HD endoscopic images are gathered using three different i-Scan modes:

- i-Scan 1 includes surface enhancement and contrast enhancement. Surface enhancement mode augments pit pattern (see Fig. 3) and surface details, providing assistance to the detection of dysplastic areas. This mode enhances light-to-dark contrast by obtaining luminance intensity data for each pixel and adjusting it to accentuate mucosal surfaces.
- i-Scan 2 includes surface enhancement, contrast enhancement and tone enhancement. Expands on i-Scan 1 by adjusting the surface and contrast enhancement settings and adding tone enhancement attributes to the image. It assists by intensifying boundaries, margins, surface architecture and difficult-to-discern polyps.
- i-Scan 3 also includes surface enhancement, contrast enhancement and tone enhancement. Similar to i-Scan 2, with increased illumination and emphasis on the visualization of vascular features. This mode accentuates pattern and vascular architecture.

In Fig. 2 we see an image showing an adenomatous polyp without image enhancement technology (a), example images using CVC (b)–(d), an image using CC (e) and images combining CC and CVC by using the i-Scan technology to visually enhance the already stained mucosa (f)–(h).

In our work we use a two-class classification scheme for our eight image databases gathered by HD endoscopy in combination with CC and the i-Scan technology. Lesions of pit pattern type I and II can be grouped into non-neoplastic lesions (healthy mucosa) and types III–V can be grouped into neoplastic lesions (abnormal mucosa). This allows a grouping of lesions into two classes, which is quite relevant in clinical practice as indicated in a study by Kato et al. (2006). In Fig. 3 we see the various pit pattern types divided into two classes (denoted as class “Healthy” and class “Abnormal”) along with exemplar images of these two classes obtained by an HD endoscope using CC and i-Scan mode 2.

One of the aims of this work is to compare classification results with respect to using CVC (i-Scan) or CC (staining). We will also examine the effects of combinations of CVC and CC on the classification results.

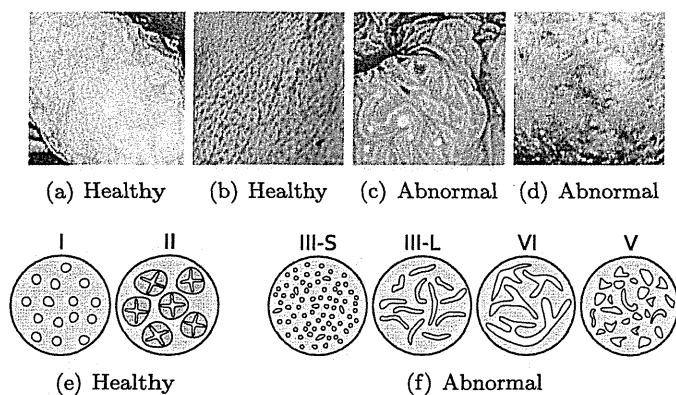


Fig. 3. Example images of the two classes (top row) and the pit pattern types of these two classes (bottom row).

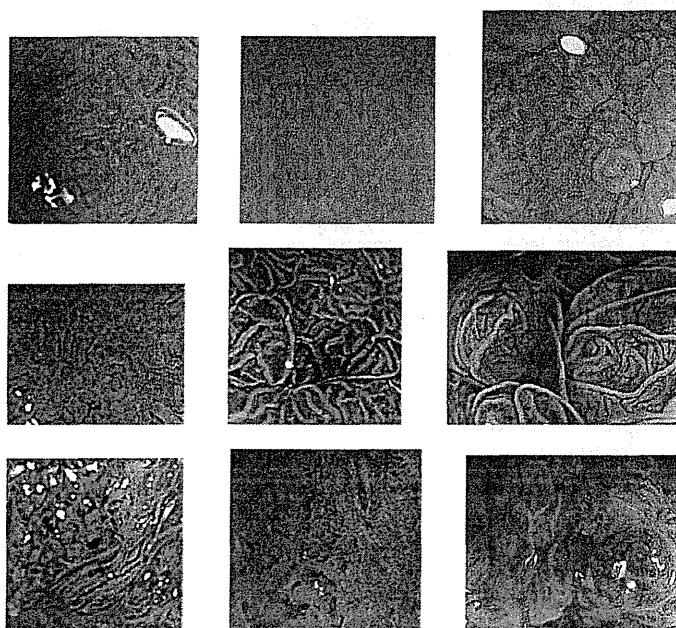


Fig. 4. Example of NBI images of types A (top row), B (middle row) and C3 (bottom row).

2.2. High-magnification endoscopy in combination with NBI

NBI (Gono et al., 2003) is a videoendoscopic system using RGB rotary filters placed in front of a white light source to narrow the bandwidth of the spectral transmittance. NBI enhances the visibility of microvessels and their fine structure on the colorectal surface. Also the pits are indirectly observable, since the microvessels between the pits are enhanced in black, while the pits are left in white. In this paper we use the classification scheme of the medical research group of the Hiroshima University Hospital (Kanao et al., 2008). This classification scheme divides the microvessel structure in an NBI image into types A, B and C. In type A microvessels are either not or only slightly observed (opaque with very low contrast). In type B, fine microvessels are visible around clearly observed pits. Type C is divided into three subtypes C1, C2, and C3. In type C3, which exhibits the most irregular texture, pits are almost invisible because of the irregularity of tumors, and microvessels are irregular and thick, or heterogeneously distorted. In Fig. 4 we see examples from the classes A, B and C3 (without CC).

It has been shown that this classification scheme has a strong correlation with histological diagnosis (Kanao et al., 2008). 80% of type A corresponds to hyperplasias and 20% to tubular adenomas. 79.7%

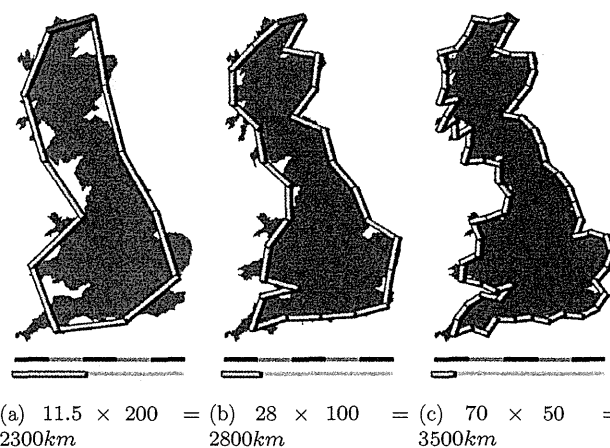


Fig. 5. As the length of the measuring stick is decreasing, the total length of the coastline measured is increasing.

of type B corresponds to tubular adenomas and 20.3% to carcinomas with intramucosal invasion to scanty submucosal invasion. 100% of type C3 correspond to carcinomas with massive submucosal invasion. Intramucosal invasion to scanty submucosal invasion (Pit Pattern type V_I) demands further examinations and carcinomas with massive submucosal invasion (Pit Pattern type V_N) requires surgery. Therefore it is important to detect type C3 among other types, instead of differentiating just between the two classes of neoplastic and non-neoplastic lesions. Like in Kanao et al. (2008) and Tamaki et al. (2013), types C1 and C2 are excluded from the experiments of this paper.

3. Local fractal dimension based feature extraction approaches

3.1. The fractal dimension

As already mentioned in the Introduction, the fractal dimension is the key quantity to describe the fractal geometry and the heterogeneity of irregular shapes. Fundamental to the fractal dimension is the concept of “measurements at scale σ ”. For each σ , we measure an object in a way that ignores irregularity of size less than σ , and we analyze how these measurements behave as σ goes to 0. A well-known example to illustrate this concept is the length of a coastline measured with differently long measuring sticks (see Fig. 5).

For most natural phenomena, the estimated quantity (e.g., the length of a coast) is proportional to $(1/\sigma)^D$ for some D . For most natural objects, D is almost the same for small scales σ . Its limit D for $\sigma \rightarrow 0$ is defined as the fractal dimension. In case of an irregular point set E defined on \mathbb{R}^2 , the fractal dimension of E is defined as

$$\dim(E) = \lim_{\sigma \rightarrow 0} \frac{\log(N(\sigma, E))}{-\log \sigma}, \quad (1)$$

where $N(\sigma, E)$ is the smallest number of sets of diameter less than σ that cover E . The set consists of closed disks of radius σ or squares of side σ . In practice, the fractal dimension is usually computed using the box counting method (dividing the space with a mesh of quadratic boxes of size $\sigma \times \sigma$, and counting the boxes occupied by the point set).

The fractal dimension D of any object in 2D space is between 0 and 2. The fractal dimensions of a point, a smooth curve or a completely filled rectangle is the same as their topological dimension (0, 1 and 2). Irregular sets have a fractal dimension between 0 and 2 (see Fig. 6). For example a curve with fractal dimension very near to 1 behaves similar to an ordinary line, but a curve with fractal dimension close to 2 winds convolutedly through space very nearly like a surface.

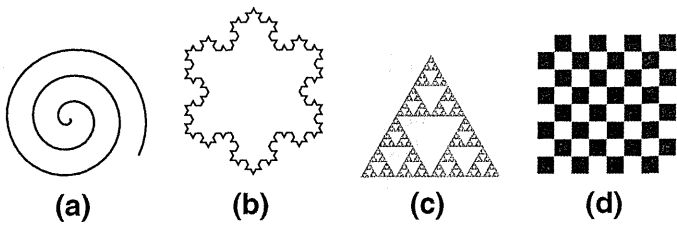


Fig. 6. Fractal dimension D in 2D space. (a) Smooth spiral curve with $D = 1$, (b) the Koch snowflake with $D \approx 1.26$, (c) the Sierpinski-Triangle with $D \approx 1.58$ and (d) the checkerboard with $D = 2$.

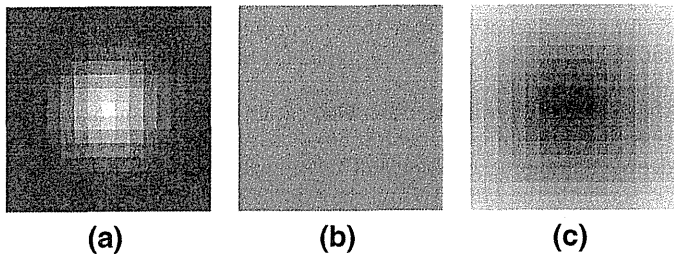


Fig. 7. LFD's at the center point using $\mu(B(x, r)) = \sum_{\|y-x\| \leq r} I(y)$: (a) LFD = 1.64, (b) LFD = 2, and (c) LFD = 2.37.

3.2. The local fractal dimension

Let μ be a finite Borel regular measure on \mathbb{R}^2 .

For $x \in \mathbb{R}^2$, denote $B(x, r)$ as the closed disk with center x and radius $r > 0$. $\mu(B(x, r))$ is considered as an exponential function of r , i.e. $\mu(B(x, r)) = cr^{D(x)}$, where $D(x)$ is the density function and c is some constant. As an example, $\mu(B(x, r))$ could be the sum of all pixel intensities that lie within a closed disk of radius r centered at an image point x , i.e. $\mu(B(x, r)) = \sum_{\|y-x\| \leq r} I(y)$.

The LFD (Xu et al., 2009) (or also called the local density function) of x is defined as

$$\text{LFD}(x) = \lim_{r \rightarrow 0} \frac{\log \mu(B(x, r))}{\log r}. \quad (2)$$

The LFD measures the “non-uniformness” of the intensity distribution in the region neighboring the considered point. In Fig. 7 we show examples of values of the LFD for different intensity distributions. If the intensities decrease from the center outward, then the center point has an LFD < 2 . For uniform intensities, the LFD = 2. Finally, if the surrounding intensities increase from the center outward, the LFD of the center point is > 2 .

In that way, the pit pattern structure of the mucosa provide high responses in terms of the LFD. Pits produce high LFD values and the peaks of the pit pattern structure produce low LFD values. So the LFD response is highlighting the pit pattern structure of the mucosa. In Fig. 8 (a) and (b) we see an image of class abnormal and its LFD's and in (c) and (d) we see an image of healthy mucosa and its LFD's (both images are gathered using an HD endoscope combined with i-Scan mode 2).

As already mentioned before, the LFD is invariant under the bi-Lipschitz map, which includes view-point changes and non-rigid deformations of texture surface as well as local affine illumination changes (Xu et al., 2009). A bi-Lipschitz function g must be invertible and satisfy the constraint $c_1 \|x - y\| \leq \|g(x) - g(y)\| \leq c_2 \|x - y\|$ for $c_2 \geq c_1 > 0$. The core of the proof in Xu et al. (2009) shows that for an bi-Lipschitz transform g applied to an image $I(x)$ with $I'(x) = I(g(x))$, the LFD of $I(x)$ and $I(g(x))$ are identical:

$$\frac{\log(c_1^2 \mu(B(x, r)))}{\log r} \leq \frac{\log(\mu(B(g(x), r)))}{\log r} \leq \frac{\log(c_2^2 \mu(B(x, r)))}{\log r}.$$

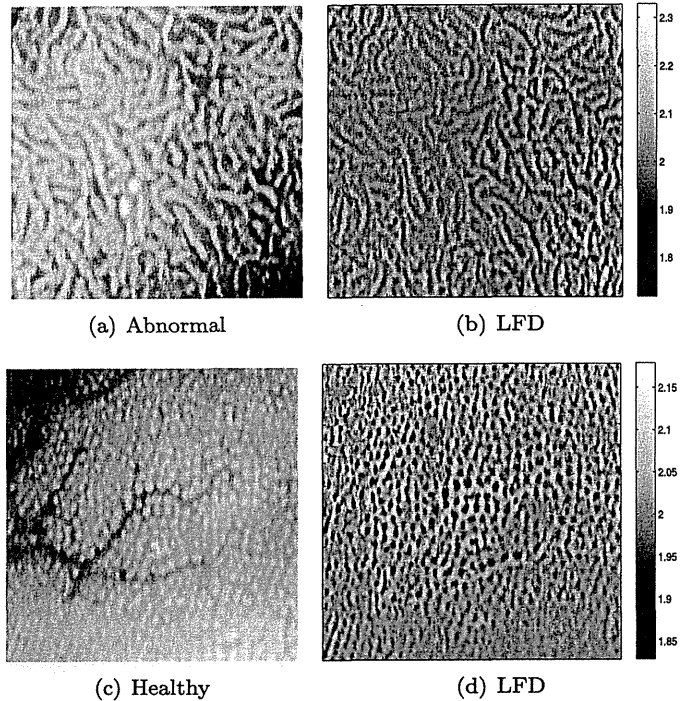


Fig. 8. Example images of class abnormal and healthy and their LFD's using $\mu(B(x, r)) = \sum_{\|y-x\| \leq r} I(y)$.

Since

$$\lim_{r \rightarrow 0} \frac{\log(c_i^2 \mu(B(x, r)))}{\log r} = \lim_{r \rightarrow 0} \frac{2 \log c_i}{\log r} + \lim_{r \rightarrow 0} \frac{\log \mu(B(x, r))}{\log r}$$

for $i \in \{1, 2\}$ and since $\frac{\log 2c_i}{\log r}$ is zero for $r \rightarrow 0$ ($\log r \rightarrow -\infty$), the fractal dimensions $D(x)$ and $D(g(x))$ are identical.

However, the proof shows that the LFD is invariant in a continuous scenario, but not in case of a discrete scenario (e.g. an image), since $r \rightarrow 0$ is not possible for an image with limited resolution. So the LFD is not proven to be viewpoint invariant in case of any image processing tasks. Of course, total viewpoint invariance in image processing tasks is impossible since images appear totally different for huge differences in scale. Despite their missing actually viewpoint invariance, the viewpoint invariance of the two approaches using the LFD (Varma and Garg, 2007; Xu et al., 2009) seems to be sufficient to achieve high classification rates on the UIUCtex database (Lazebnik et al., 2005), a texture database consisting of texture images which are acquired under quite different viewpoint conditions.

In practical computation, the LFD at each pixel location x of an image is computed by linear fitting the slope of the line in a scaling plot of $\log \mu(B(x, r))$ against $\log r$ for $r = \{1, \dots, 8\}$. In Fig. 9, we visually show the computation of the LFD for the pixel location x of an image I using $\mu(B(x, r)) = \int_{B(x, r)} I(x) dx = \sum_{\|y-x\| \leq r} I(y)$.

3.3. Feature extraction methods based on the LFD

3.3.1. The MFS-LFD approach

In the approach of Xu et al. (2009), three different definitions of $\mu(B(x, r))$ are used, which capture different aspects of the structure of textures:

$$\mu_1(B(x, r)) = \int_{B(x, r)} I(\sigma) dx \quad (3)$$

$$\mu_2(B(x, r)) = \int_{B(x, r)} \sum_{k=1}^4 (f_k * (I(\sigma)^2))^{\frac{1}{2}} dx \quad (4)$$

$$\mu_3(B(x, r)) = \int_{B(x, r)} |I_{xx}(\sigma) + I_{yy}(\sigma)| dx, \quad (5)$$

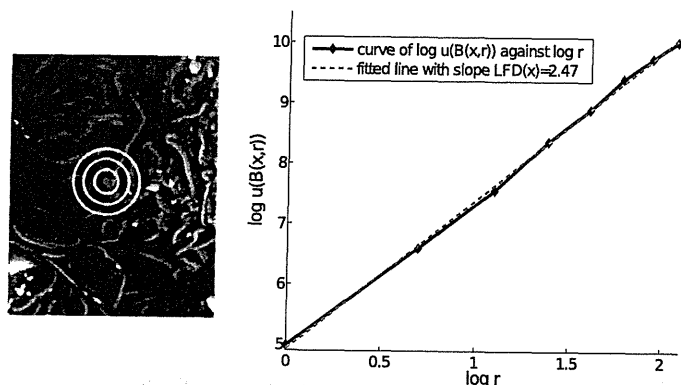


Fig. 9. In the image to the left we see the schematic representation of a pixel location x (orange dot) and the corresponding disks $B(x, r)$ (yellow). The plot to the right visually shows the computation of the LFD by linear fitting the slope of the line of $\log \mu(B(x, r))$ against $\log r$. (For interpretation of the references to color in this figure legend, the reader is referred to the web version of this article.)

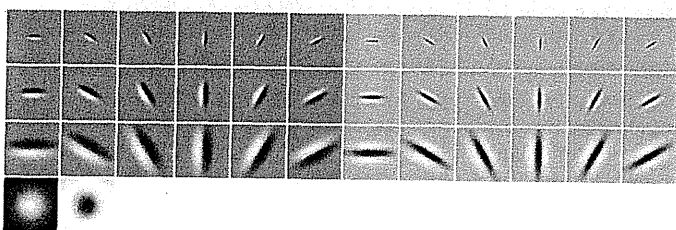


Fig. 10. The filters of the MR8 filter bank.

where $I(\sigma)$ is the Gaussian blurred image I using variance σ^2 , $I_{xx}(\sigma)$ is the second derivative in x -direction, “ $*$ ” is the 2D convolution operator and $\{f_k, k = 1, 2, 3, 4\}$ are four directional operators (derivatives) along the vertical, horizontal, diagonal, and anti-diagonal directions.

Let E_α be the set of all image points x with LFD's in the interval α :

$$E_\alpha = \{x \in \mathbb{R}^2 : \text{LFD}(x) \in \alpha\}.$$

Usually this set is irregular and has a fractional dimension $f(\alpha) = \dim(E_\alpha)$. The feature vector of an image I consists of the concatenation of the fractal dimensions $f(\alpha)$ for the three different measures $\mu_k(B(x, r))$, $k \in \{1, 2, 3\}$.

That means the range of values of the LFD's is splitted into N equally sized intervals α_i , $i \in \{1, \dots, N\}$ ($N = 26$ in Xu et al., 2009). So for each of the three measures $\mu_k(B(x, r))$, we generate 26 binary images $I_b^{\alpha_i}$, where $I_b^{\alpha_i}(x, y) = 1$ if $\text{LFD}(x, y) \in \alpha_i$ and $I_b^{\alpha_i}(x, y) = 0$ otherwise. The final feature vector consists of the fractal dimensions of the 26 binary images per measure $\mu_k(B(x, r))$. So the feature vector of an image consists of $3 * 26 = 78$ features per image. We furtherly denote this approach as the multi fractal spectrum LFD (MFS-LFD) approach.

3.3.2. The MR8-LFD approach

In the approach presented in Varma and Garg (2007), the images are convoluted with the MR8 filter bank (Geusebroek et al., 2003; Varma and Zissermann, 2005), a rotationally invariant, nonlinear filter bank with 38 filters but only eight filter responses. It contains edge and bar filters, each at six orientations and three scales, as well as a rotationally symmetric Laplacian and Gaussian filter (see Fig. 10). Rotation invariance is achieved by taking only the maximum response over all orientations for each scale of the edge and bar filters.

The LFD's are computed for each of the eight filter responses $f_i(I)$, $i \in \{1, \dots, 8\}$ using the measure

$$\mu(B(x, r)) = \int_{B(x, r)} |f_i(I)| dx.$$

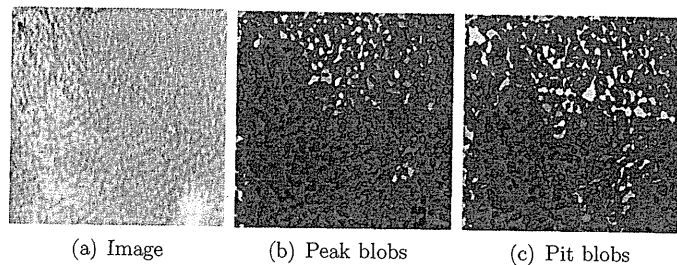


Fig. 11. The extracted peak and pit blobs of the image.

So for each pixel of an image there is an eight-dimensional LFD vector. Finally, the BoW approach is applied to the LFD vectors. The visual words are learned by k -means clustering the LFD vectors using 100 cluster centers per image class. The feature vector of an image consists of the resulting histograms of the BoW approach. We furtherly denote this approach as the MR8-LFD approach.

For both, the MFS-LFD and the MR8-LFD approach, disks $B(x, r)$ with $r = \{1, \dots, 8\}$ are used to sum the intensity values $I(y)$ (where $I(y)$ is the Gaussian blurred image $I(\sigma)$, the gradient image or the Laplacian of the image in case of the MFS-LFD approach and one of the eight MR8 filter responses in case of the MR8-LFD approach) surrounding the considered pixel x with $\|x - y\| \leq r$. We can interpret these disks as circle shaped binary filters, with which the image (respectively its filter responses or its derivatives) is filtered.

3.3.3. The blob-adapted LFD approach

In Häfner et al. (2014c), we proposed a feature extraction method that is derived from the LFD. However, instead of disk shaped filters with preassigned radii ($B(x, r)$), we used ellipsoidal binary filters and anisotropic, ellipsoidal Gaussian filters fitted to the shape, size and orientation of the local texture structure. The shapes, orientations and sizes of the filters are adapted to the shapes, orientations and sizes of connected components (blobs).

These blobs are generated by a segmentation algorithm (Häfner et al., 2014c), that applies local region growing to the maxima and minima of the image in a similar way as the watershed segmentation by immersion (Roerdink and Meijster, 2000; Vincent and Soille, 1991).

The blobs represent the local texture structures of an image. We differentiate between blobs evolved from local minima (pit blobs) and blobs evolved from local maxima (peak blobs) of an image (see Fig. 11). Roughly said, beginning with a local minima (maxima), the algorithm adds those neighboring pixels to the considered minima (maxima), which have the smallest (highest) intensity value of all neighboring pixels. In this way we generate a blob and this blob is growing as long as the darkest (brightest) neighboring pixel of the blob is brighter (darker) or equally bright (dark) as the brightest (darkest) pixel of the blob. If the darkest (brightest) neighboring pixel is darker (brighter) as the brightest (darkest) pixel of the blob, the region growing algorithm stops resulting in a pit (peak) blob b evolved from the local minima (maxima).

The idea behind this segmentation approach is that different classes of polyps have different typical pit pattern types (see Fig. 3). By filling up the pits and peaks of a mucosal image, the resultant blobs represent the shapes of local structures of the image including the different types of pit pattern. In that way the shape of the blobs contain information that enables a distinction between healthy and abnormal mucosa (see Häfner et al., 2014a).

For further feature extraction (computing the LFD derived feature), only the blobs with $N \geq 8$ pixels are used. In this way it is ensured that only these blobs are used which represent a distinct pit or peak and exclude those blobs which evolve of minima or maxima that are caused by noise. For each resulting blob, the inertia matrix

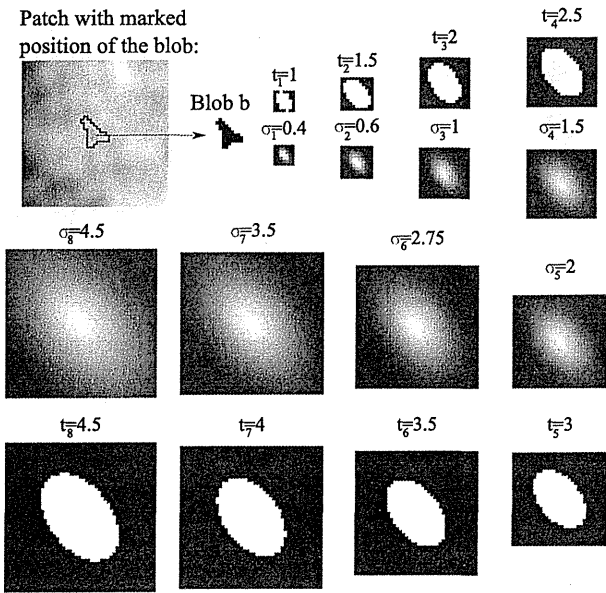


Fig. 12. A patch containing a blob b in his center and the corresponding binary elliptic filter masks $E_b^{t_i}$ and elliptic Gaussian filter masks $G_b^{\sigma_i}$.

is computed and from these matrices we determine the eigenvectors and eigenvalues.

The orientation and shape of an elliptic filter is derived from the eigenvectors and eigenvalues of the inertia matrix of a blob. That means for each blob b , a specific filter is generated and its shape and orientation is adapted to the considered blob. The size of the elliptic filters is adapted to the number of pixels of the corresponding blob (the higher the number of pixels, the bigger the size of the filter).

Like in the two previous approaches, eight differently sized binary filters are used (disks $B(x, r)$ with $r = \{1, \dots, 8\}$ in case of the previous approaches). The size of the eight elliptic binary filters is controlled by eight threshold parameters $t_i \times \sqrt{N/\pi}$, $i \in \{1, \dots, 8\}$ (t_i , $i \in \{1, \dots, 8\}$ is fixed and strictly monotonic increasing and N is the number of pixels of the considered blob). Additionally to the eight binary filters $E_b^{t_i}$, eight Gaussian filters are used, whose shape and orientation is equally determined as for the binary filters. Instead of the threshold parameters t_i , eight standard deviations $\sigma_i \times \sqrt{N/\pi}$, $i \in \{1, \dots, 8\}$ are used as size-perimeters for the Gaussian filters $G_b^{\sigma_i}$ (see Häfner et al., 2014c), where σ_i , $i \in \{1, \dots, 8\}$ is fixed and strictly monotonic increasing.

The parameters t_i and σ_i are chosen so that the filters uniformly gain in size with increasing i .

In Fig. 12 we see an image patch containing a blob b and the corresponding binary and Gaussian filters.

For a given Blob b with center position (\bar{x}, \bar{y}) in the image I and the corresponding filters $G_b^{\sigma_i}$ ($E_b^{t_i}$ analogous) with filter size $f \times f$, μ is defined as follows:

$$\mu(G_b^{\sigma_i}) = \sum_{x=-\frac{f-1}{2}}^{\frac{f-1}{2}} \sum_{y=-\frac{f-1}{2}}^{\frac{f-1}{2}} I(\bar{x}-x, \bar{y}-y) G_b^{\sigma_i}(x, y)$$

The LFD derived features are computed separately for binary and Gaussian filters and only for interest points, which are defined as the centers of the blobs. The two LFD derived features for a blob b are defined as:

$$\text{LFD}_E(b) = \lim_{i \rightarrow 0} \frac{\log \mu(E_b^{t_i})}{\log i}, \quad \text{LFD}_G(b) = \lim_{i \rightarrow 0} \frac{\log \mu(G_b^{\sigma_i})}{\log i}, \quad (6)$$

where σ_i and t_i are strictly monotonic increasing. Equally to the original LFD, the practical computation of the LFD_E (LFD_G) is done by linear

fitting the slope of the line in a scaling plot of $\log \mu(E_b^{t_i})$ ($\log \mu(G_b^{\sigma_i})$) against $\log i$ with $i \in \{1, \dots, 8\}$.

Since the two features LFD_E and LFD_G in this approach are derived from the LFD as defined in the two previous approaches (MFS-LFD and MR8-LFD), we will further denote them as blob-adapted LFD (BA-LFD).

The BA-LFD measures the “non-uniformity” of the intensity distribution in the region and neighboring region of a blob. Starting with the center region of a pit or peak, it analyzes the changes in the intensity distribution with expanding region. In that way it analyzes the changing intensity distribution from the inside to the outside of a pit or peak in an image. Since size, shape and orientation of the filters are adapted to the blob representing the pit or peak, the BA-LFD should be even more invariant to varying viewpoint conditions as the LFD using disks with fixed radii (Xu et al., 2009).

The BA-LFD approach was especially designed to classify polyps using the CC-i-Scan databases. It finds the pits and peaks of the pit pattern structure and then filters the area in and surrounding the detected pits with filters that are shape, size (= scale) and orientation adapted to the pits and peaks.

The final feature vector of an image consists of the concatenation of the histograms of the LFD_E 's separately computed for the pit and peak blobs of an image and the histograms of the LFD_G 's separately computed of the pit and peak blobs of an image. Each of the four histograms consists of 15 bins. All parameter values (e.g., the number of bins per histogram, σ_i and t_i) are taken from the original approach (Häfner et al., 2014c).

Distances between two feature vectors are measured using the χ^2 statistic, which has been frequently used to compare probability distributions (histograms) and is defined by

$$\chi^2(x, y) = \sum_i \frac{(x_i - y_i)^2}{x_i + y_i}. \quad (7)$$

Also the three extensions of the BA-LFD approach (see Section 3.5) use the χ^2 statistic as distance metric. The histograms of the BA-LFD approach (and its three extensions) are not normalized. In case of the experiments using the NBI database, the values of the histograms of an image are divided by the number of pixels of the considered image, to balance the different sizes of the NBI images. This approach will be further denoted as the BA-LFD approach.

3.4. Closing the gap between LFD and BA-LFD

As already mentioned before, there are major differences between the LFD and the BA-LFD. Contrary to the LFD, the filters of the BA-LFD are

- scale-adapted by fitting the size of the filters to the number of pixels per blob,
- shape and orientation-adapted by fitting the shape and orientation of the filters to the shape and orientation of the blobs,
- only applied on interest points, which are defined as the centers of peak and pit blobs that are detected by a segmentation algorithm,
- partly Gaussian filters and partly binary filters (instead of only binary filters).

To analyze the weak and strong points of the BA-LFD compared to the LFD and to analyze which of the adaptations make sense and which not, we will create methods that are intermediate steps between the LFD and the BA-LFD. That means we leave out one or several of the four adaptation steps that turn the LFD into the BA-LFD. For a better comparability of the results, for each intermediate step the histograms of the LFD's (or BA-LFD's) are used as features. It should be noted that the computation of LFD's (BA-LFD's) only on interest points means that we separately compute histograms of the LFD's